Torsion-Driven Plectoneme Formation During Nanopore Translocation of DNA Polymers

Fei Zheng,[1,2,3] Antonio Suma,[4] Christopher Maffeo,[5] Kaikai Chen,[2] Mohammed Alawami,[1] Jingjie Sha,[3] Aleksei Aksimentiev,[5] Cristian Micheletti,[6,*] and Ulrich F. Keyser[1,†]

[1]*Cavendish Laboratory, University of Cambridge, Cambridge CB3 0HE, United Kingdom*
[2]*School of Nanoscience and Nanotechnology, University of Chinese Academy of Sciences, 101408 Beijing, China*
[3]*Jiangsu Key Laboratory for Design and Manufacture of Micro-Nano Biomedical Instruments, School of Mechanical Engineering, Southeast University, 211100 Nanjing, China*
[4]*Dipartimento Interateneo di Fisica, Università degli Studi di Bari and INFN, Sezione di Bari, I-70126 Bari, Italy*
[5]*Department of Physics, University of Illinois at Urbana–Champaign, Urbana, Illinois 61801, USA*
[6]*SISSA—Scuola Internazionale Superiore di Studi Avanzati, I-34136 Trieste, Italy*

(Received 3 July 2024; revised 8 May 2025; accepted 20 May 2025; published 12 August 2025)

The transport of DNA polymers through nanoscale pores is central to many biological processes, from bacterial gene exchange to viral infection. In single-molecule nanopore sensing, the detection of nucleic acid and protein analytes relies on the passage of a long biopolymer through a nanoscale aperture. Understanding the dynamics of polymer translocation through nanopores, especially the relation between ionic current signal and polymer conformations, is thus essential for the successful identification of targets. Here, by analyzing ionic current traces of dsDNA translocation, we reveal that features up to now uniquely associated with knots are instead different structural motifs: plectonemes. By combining experiments and simulations, we demonstrate that such plectonemes form because of the solvent flow that induces rotation of the helical DNA fragment in the nanopore, causing torsion propagation outwards from the pore. Molecular dynamic simulations reveal that plectoneme nucleation is dominated by the applied torque, while the translocation time and size of the plectonemes depend on the coupling of torque and pulling force, a mechanism that might also be relevant for *in vivo* DNA organization. Experiments with nicked DNA constructs show that the number of plectonemes depends on the rotational constraints of the translocating molecules. Thus, our work introduces plectonemes as essential structural features that must be considered for accurate analysis of dsDNA polymers in the nanopore.

DOI: 10.1103/spyg-kl86

Subject Areas: Biological Physics, Nanophysics, Soft Matter

I. INTRODUCTION

The rapid analysis of biopolymers like DNA is a major goal in many biosensing applications [1]. With nanopore sensing, the length and three-dimensional shape of a translocating molecule are extracted from the ionic current signal [2]. Topological conformations like knots or other complex structures are increasingly recognized as crucial targets of single-molecule biosensors for monitoring cellular functions [3–9]. DNA sequencing using nanopore sensors [10] has found numerous applications; however, in such setups, translocation is controlled by molecular motors [11–13] that unzip DNA and remove 3D entangled motifs like knots and plectonemic supercoils from the sequenced strand. In contrast, larger solid-state nanopores have revealed the dynamics of double-stranded DNA (dsDNA) polymers as they traverse through nanoscale confinements since the early 2000s [14–20]. Generally, voltage-driven DNA translocation through a nanopore is often simply described as a quasi-one-dimensional movement with the force applied in the direction of the double helix [21–24]. However, dsDNA in the usual B-form has a right-handed helical structure; thus, additional rotational forces were recently observed in experiments and simulations [25–27]. Simply put, the ionic current transfers momentum to the water molecules in the nanopore, which results in a torque on the dsDNA. Accordingly, the DNA helix starts to rotate. The additional torque should lead to a rotational movement with consequences beyond the usual picture of simple, force-driven electrophoretic translocation.

Electrophoretically driven translocation is a process that proceeds far from equilibrium. Especially in experiments

*Contact author: michelet@sissa.it
†Contact author: ufk20@cam.ac.uk

where the DNA length is much greater than the nanopore diameter and length [28–30], the dynamics of the DNA segments outside the nanopore influence the translocation process [31]. The translocation time is often so fast that the DNA conformation in front of the nanopore cannot relax during translocation. Effects like tension propagation have been studied both in simulations [31–35] and experiments [14], where a direct consequence of the rapid pulling of the molecules through the nanopore is the possibility to trap, and hence study, topological structures like knots [22,36], which are statistically inevitable and yet generally detrimental to the cell functioning [37–40]. Knots form stochastically outside the pore where the DNA strand self-entangles [41–43]. When one end of the DNA strand is electrophoretically pulled into the pore, tension propagates along the strand to the outer part, causing the knot to tighten and ultimately facilitating its translocation [36,41,44]. A characteristic current signature of knots includes a secondary transient spike in addition to the current blockade induced by the linear strand [22,36,45]. Typically, the ionic current signal in a nanopore is translated into the number of strands in the sensing volume. For the simplest trefoil knot, three dsDNA strands pass the nanopore at the same time, and hence the total current amplitude of the knotted signal is 3 times that of the single dsDNA strand current level. More complex knots have been observed in experiments, but there is no clear consensus on the exact shape of the knots [22,36].

Here, we use the recent discovery that DNA helix structures experience significant torque and hence rotation during out-of-equilibrium nanopore translocation [26] and harness it to assign numerous ionic current traces to plectonemic structures in addition to well-characterized knots. Plectonemes refer to a twisted DNA structure in which the dsDNA strand coils onto itself into a looplike shape. We present careful measurements of DNA translocation as a function of DNA length, voltage, and torsional constraints. We find that the torsion generated by in-pore electro-osmotic flow likely propagates along the strand to the outer DNA segments, which in turn twist the strand into plectonemes. A combination of experiments and simulations indicates that plectonemes can be pulled into the nanopore with three or more dsDNA strands moving inwards concurrently. Our molecular dynamics simulations reveal intricate physical features of plectoneme dynamics during nanopore translocation. Furthermore, we design nicked DNA structures to show the crucial role of torsional constraints for the formation of plectonemes in the DNA double helix.

II. KNOTS OR PLECTONEMES OR BOTH IN NANOPORES

A schematic of the experiment is shown in Fig. 1(a). A dsDNA molecule (red) is pulled through a conical nanopore by the applied positive potential. The nanopore is large enough (about 14 nm in diameter) to allow for the passage of more than one DNA strand. Three possible conformations with three DNA strands side by side are shown in the sketch—the supercoil, the figure-eight knot, and the "S"-shape fold. All three structures lead to the same ionic current signal, as shown in the example trace in Fig. 1(b). In this signal, we indicate four levels: the baseline 0, the double-stranded DNA level 1, the folded DNA level 2 (not shown in this example), and finally, the triple strand level 3 that could represent any of the three structures in Fig. 1(a). We obtain these current levels from the distributions of an all-current-point histogram (Figs. 3–6 of the Supplemental Material [46]). As the knot is only one of the explanations for the level 3 signal, we call the events of all those possible conformations "tangled." In the following, we define the "tangling probability" as the number of tangled events divided by the total number of nanopore events.

We measure the tangling probability in a single nanopore for DNA of 2, 5, 10, 15, 20, and 48.5 kbp in length [blue diamond, Fig. 1(c)]. Following previous results [36], we calculate the tangling probability initially attributing all "$\geq$3" events to knots. The tangling probability increases with DNA length, which is expected as longer molecules should exhibit more knots. For 48.5-kbp long lambda DNA, we obtain a tangling probability of 62.6%. In other words, approximately two out of three translocation events are tangled. The two red lines in Fig. 1(c) show the equilibrium knotting probabilities of DNA molecules at given lengths calculated using Monte Carlo simulations (Note 6 of Ref. [46]). The data are for two sets of DNA structural parameters compatible with the experiments, including the cross-sectional diameter, d, and the persistence length, lp (see Fig. 7 of Ref. [46] for additional conditions). For reference, the simulated knotting probabilities of lambda DNA are 25.7% and 25.3% for lp of 40 nm and 50 nm, respectively.

Figure 1(c) shows a substantial difference between the measured tangling probability (blue symbols) and the calculated maximum knotting probability, a difference that becomes even larger as the DNA length increases. For 48.5-kbp DNA, the tangling probability is more than double the knotting probability, with the absolute difference running up to 37%. Note that the calculated equilibrium knotting probability provides an upper bound for the number of knots detectable via a nanopore translocation measurement [47], as such detectable knots can only originate from self-entanglement of the DNA before the translocation measurement and with no additional knots forming during the translocation process [22,36,48]. In fact, the voltage-driven translocation minimizes knot formation in the probed DNA portion—the one on the *cis* side—due to several concurrent effects. On the one hand, the rapid DNA translocation (around 10 ms) limits the opportunity for DNA strands to self-entrain into complex topological states such as knots. The latter is further suppressed by the fact that translocation progressively

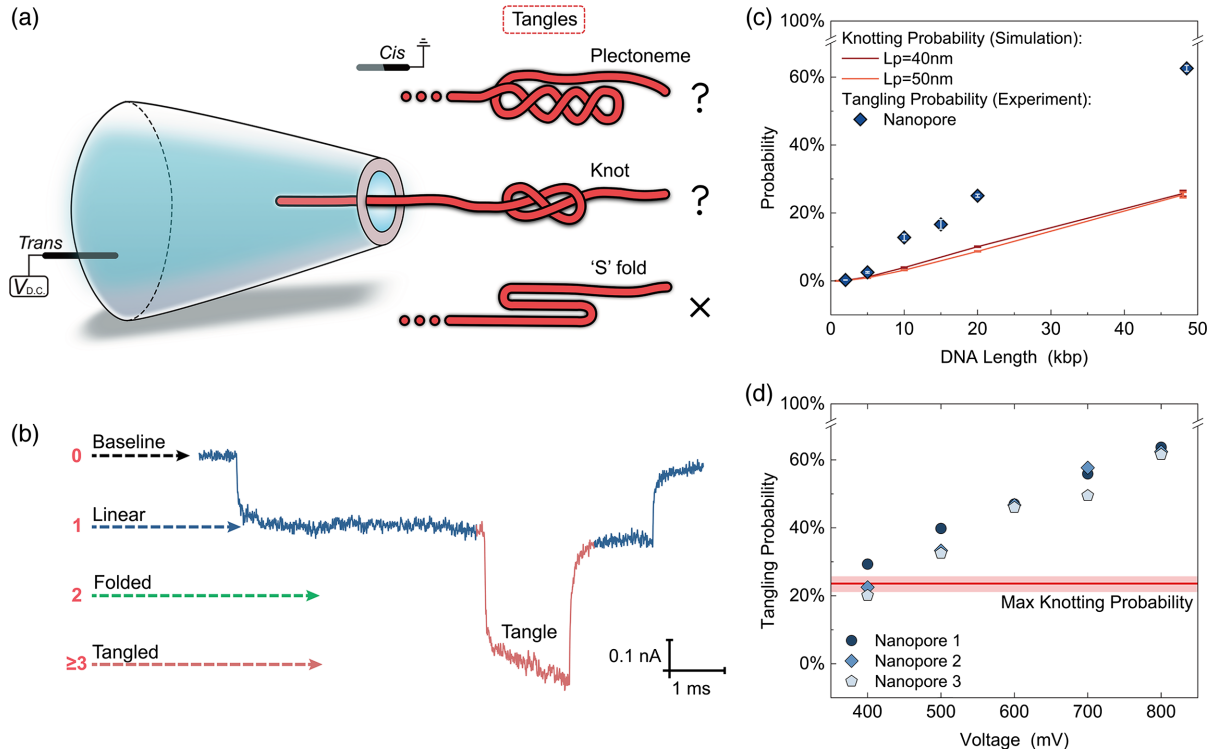

FIG. 1. Tangling probability higher than the theoretical knotting probability. (a) Schematic of three tangled conformations, including the plectoneme, the knot, and the S shape, moving through a nanopore. (b) Ionic current signal from typical tangled events categorized according to four current levels: 0—current baseline; 1—linear (single dsDNA strand) translocation; 2—folded (two dsDNA strands) translocation; ≥ 3—tangled (equal to or more than three dsDNA strands) translocation. The ionic current trace is from a 48.5-kbp lambda DNA translocating through a 14 ± 3-nm [mean ± standard deviation (s.d.)] diameter pore under an applied voltage of +800 mV. The cone semiangle of this nanopore is 0.05 ± 0.01 radians (mean ± s.d.) based on previous characterization [15]. (c) Comparison of the experimentally measured tangling probability (≥ 3 events) and the equilibrium knotting probability calculated using Monte Carlo simulations. Each diamond symbol shows the experimentally measured tangling probability averaged over three nanopores for the DNA ladder (2, 5, 10, 15, 20, and 48.5 kbp). The two lines indicate the simulated knotting probability for the DNA ladder (2, 5, 10, 15, 20, and 48 kbp), differing by the assumed persistence length, lp, value: 40 nm or 50 nm and effective dsDNA diameter of 2.0 nm. The enlarged views of the 2- and 5-kbp values are provided in Fig. 7 of Ref. [46]. (d) Tangling probabilities (lambda DNA) as a function of applied voltage measured in three same-sized nanopores. The horizontal red line is the maximum knotting probability calculated from Monte Carlo simulations for a broad range of lp and d values.

straightens the *cis* DNA and hence reduces its effective density, while loop structures are dragged to the pore and unwound away from the free end, which is reached last by the mechanical tension propagating from the pore. This process establishes a situation that is starkly different from the one realized in nanodozer setups [49,50], where hydrodynamic compression makes it possible for the DNA ends to thread through the densely packed DNA bundle, leading to knot formation. The actual experimental knotting probability is expected to be lower than the reference equilibrium value because the knots can slide along and off the DNA during the nanopore translocation without even producing the expected ionic current signature [36,41,44,51]. Hence, we can conclude that the tangled level greater than or equal to 3 can not only be knots and must be either the S shape or the plectonemes, Fig. 1(a).

Next, we examine how the tangling probability (events with levels greater than or equal to 3) in the longest DNA (48.5 kbp) changes with the applied voltage. Figure 1(d) shows that the tangling probability increases with the voltage well above the maximum equilibrium knotting probability of lambda DNA (about 25%, red line) and that the rate of the increase is consistent among the measurements conducted using different nanopores (blue symbols). In other words, the experimental tangling probability is in the range of the maximum knotting probability only at 400 mV, and it increases from about 35% to more than 60% in the 500 to 800 mV range. This voltage-dependent behavior strongly suggests that the number of tangled events cannot be fully accounted for by the expected knotting probability as higher pulling forces cannot create additional knots. Furthermore, the contribution of S structures can also be ruled out as faster translocations are expected to readily unfold the S structures by the propagated tension [36]. Hence, we hypothesize that the

excess tangling (≥3 event) probability originates from the formation of plectonemes.

III. PLECTONEMES NOT ONLY KNOTS

In the nanopore field, the possibility of plectoneme formation has so far been overlooked as DNA rotation was usually ignored. Recently, the ionic flow in nanopores was shown to empower sustained rotation of DNA helix structures at torques of approximately 0.5 pN nm per bp at 100 mV nm^{-1}, which is close in magnitude to the torque generated by RNA polymerase to produce supercoils [26,52]. Our conical nanopores are immersed in a highly alkaline solution (pH = 9), and the electro-osmotic flow is significantly enhanced (flow rate ∼50 $\mu m^3 s^{-1}$) [53,54]. Thus, we believe the electro-osmotic flow in our conical nanopore is sufficient to generate a torque that twists the dsDNA strand and leads to the formation of plectonemes during the translocation process.

The sketches in Figs. 2(a)–2(c) illustrate how a plectoneme nucleates and then translocates. The axial electro-osmotic flow is redirected when it interacts with the DNA helix, imparting a tangential force that produces a torque on the DNA strand [Fig. 2(c)]. As the translocation proceeds much faster than relaxation of the DNA configuration, the torque subsequently propagates outwards from the nanopore along the strand, which in turn forces the outside segment to rotate about its helical axis. As shown in Fig. 2(a), the fluid friction interacting with the DNA helix leads to a torque that twists the DNA and may lead to the formation of plectonemes. Meanwhile, the electrophoretic force pulls the rest of the DNA strand into the pore, eventually translocating the plectoneme [Fig. 2(b)].

The successful translocation of plectonemes relies on the cooperation of electrophoretic force and electro-osmotic flow, which are linked in the nanopore. Importantly, the torque depends on the applied voltage, and hence we expect that there are more plectonemes forming when the voltage is increased. Figure 2(d) shows a typical nanopore signal of the plectoneme indicated by the extended level 3 in this example event. The translocation time of a plectoneme inside the pore can reach the scale of milliseconds, which is

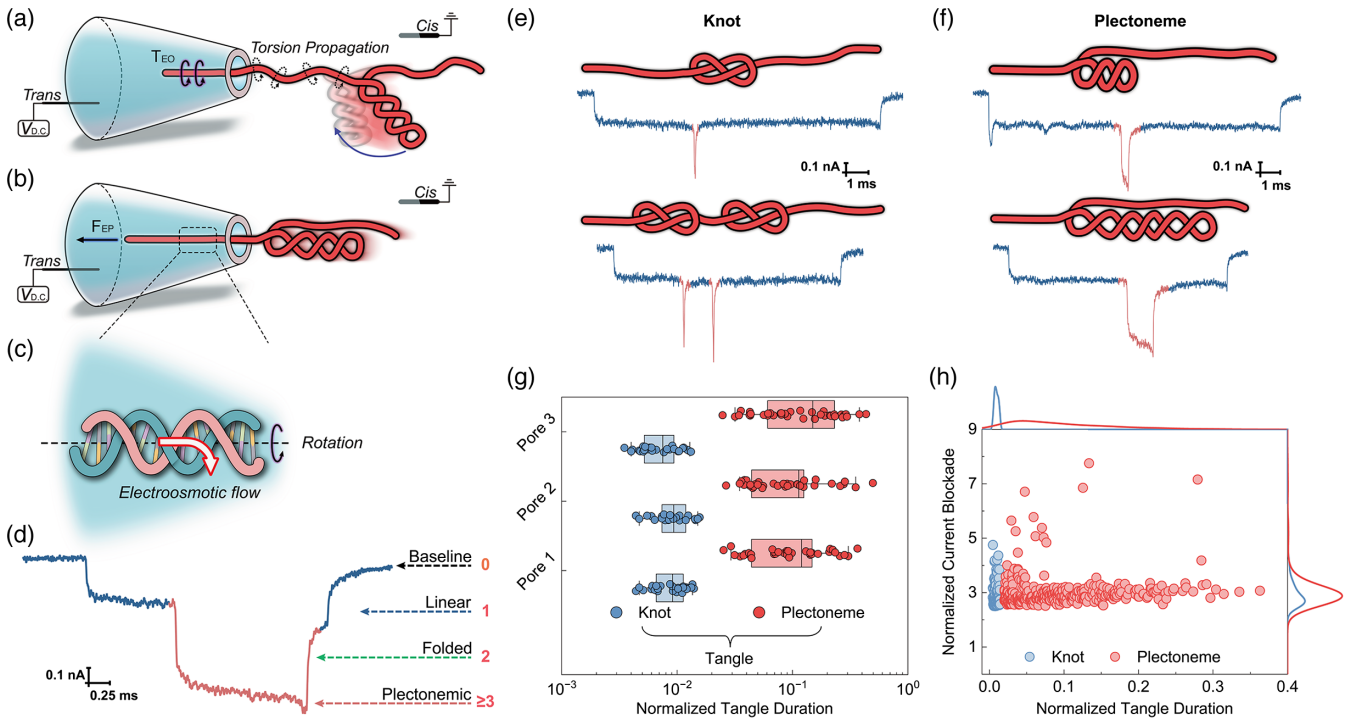

FIG. 2. Plectonemes as long tangled events. (a) Schematic of the plectoneme formation. A dsDNA strand rotates inside the pore driven by the flow-induced torque. This in-pore torsion propagates to the outside segments of the strand and forces the strand to coil on itself, thus forming a plectoneme. (b) Schematic of the plectoneme translocation. Pulled by the electrophoretic force, the plectoneme and another part of the longer molecule are threaded into the nanopore, featuring concurrent translocation of three dsDNA strands. (c) Origin of the torque. The helical structure deflects the axial electro-osmotic flow, the tangential component of which generates the rotation torque. Here, T_{EO} denotes the electroosmosis-generated torque, and F_{EP} represents the electrophoretic force. (d) Representative translocation signal of a plectoneme event. (e) Examples of knot conformation and corresponding nanopore signals. (f) Examples of plectoneme conformation and corresponding nanopore signals. (g) Comparison of the normalized duration of events associated with knots and plectonemes. The statistics are collected from the nonfolded events comprised of a knot or a plectoneme measured in three same-sized nanopores. (h) Scatter plot of normalized current blockade (the level, I_{tangle}/I_{linear}) versus normalized tangle duration for knots and plectonemes.

at least 1 order of magnitude longer than that of a knot, typically less than 100 μs, both observed in our nanopore and previous studies [36]. Figure 2(e) shows typical current blockade signatures that we associate with knotted molecules in our nanopore experiments. In contrast, typical events associated with the plectoneme passage have much longer durations, Fig. 2(f).

We can thus categorize the tangled events as knots or plectonemes based on the difference in their translocation timescales. Figure 2(g) illustrates the normalized duration of tangled events, defined as the ratio of the tangled event duration to the total duration of the translocation process. Knot signatures are short in duration and appear as a fleeting spike because knots are tightened by the propagated tension [Fig. 2(e)]. In contrast, the duration of a plectoneme signal is expected to vary according to the accumulated twist, and indeed, we observe a wide range of single durations for plectonemes, as illustrated by the examples in Fig. 2(f). Knowing the total length of the molecules, we can roughly convert the even duration into a tangle size. The knots have an estimated average size of about 140 nm whereas plectonemes are much larger, about 2100 nm (Fig. 8 of Ref. [46]). Higher-order (hence large-sized) prime knots are rare at the considered DNA lengths (Fig. 17 of Ref. [46]). As noted above, translocating knots are typically small because they are tightened by tension propagating outwards from the nanopore [51]. In contrast, plectonemes can grow to much larger sizes due to the torque being continuously applied during translocation. The DNA twist introduced by the torque is only partially unraveled by the propagating tension and thus accumulates in the form of extended plectonemes. The experimental knotting probability exhibits a slight decrease with the applied voltage (Fig. 9 of Ref. [46]) and is always below the simulation-predicted maximum knotting probability, due to knot sliding off the DNA filament.

Finally, we investigate the complexity of the plectonemic conformations. Figure 2(h) shows the scatter distribution of normalized tangle duration versus normalized current blockade for knots and plectonemes. While most knot and plectoneme events distribute at level 3, a few appear at levels 5 and 7. Some short-duration events are close to level 4, which we attribute to the limited temporal resolution of our nanopore measurement. Consistent with the equilibrium knot spectrum, and in line with previous research [22,36], we see complex knots in the nanopore signals, such as twin knots, high-order knots, and knots on a folded strand (Figs. 10, 12, and 17 of Ref. [46]). For plectonemes, we also observe complex plectonemic conformations like a knot on a plectoneme and a complex of plectonemes (Figs. 11 and 13 of Ref. [46]).

The nanopore shape—whether conical or cylindrical—exerts minimal influence on plectoneme formation in the *cis* reservoir. In addition to the above-mentioned asymmetric conical nanopores pulled from glass pipettes, we conduct experiments with membrane nanopores fabricated in Si_3N_4 membranes. In both systems, we observe clear evidence of plectonemes and knots in the translocation signals (see Note 9 and Figs. 21–24 of Ref. [46]).

IV. REPRODUCING PLECTONEME FORMATION IN MOLECULAR DYNAMICS SIMULATIONS

We performed molecular dynamics simulations of 8-kbp DNA translocation using the validated implicit-solvent model of Ref. [55], where DNA is coarse grained as a twistable elastic discrete chain [56]. The DNA portion in the pore region was simultaneously subject to a longitudinal translocating force and a torque. The pore size and the magnitude of the applied forces were selected consistent with experiments [Fig. 3(a) and Note 2 of Ref. [46]]. Hundreds of translocation trajectories were collected for different initial equilibrium conformations of the 8-kbp-long strands, with and without knots. The trajectories were analyzed to identify the passage of tangles through the pore [Figs. 3(b) and 3(c)]; the steric exclusion model [57,58] (SEM, Note 8 of Ref. [46]) was used to compute the ionic current blockade from the pore occupation [Fig. 3(d)]. Similar to experiment, the simulated current blockade resulting from a plectoneme translocation through a nanopore was found to exhibit the level 3 signal.

The top panel of Fig. 3(e) shows the percentage of unknotted DNA trajectories presenting at least one tangle event, i.e., greater than or equal to 3 strands passing through the pore, as a function of the torque and for different translocation forces, starting from initial conformations that were unknotted and torsionally relaxed, hence free of plectonemes. *A posteriori* analyses and direct inspection of the level "≥ 3" events revealed the absence of all tangle types in Fig. 1(a) except for plectonemes, confirming that the observed events are associated with the passage of intertwined superstructures formed during translocation. In contrast, knot tangles could be observed only in trajectories where the starting conformation was itself knotted because the translocation process is too short to allow the chain to relax and change its initial topological state. The durations of the knot signals was much shorter than those of plectonemes, again consistent with the experimental observations (Fig. 2; Ref. [46], Fig. 20). Because of their more complex compound entanglement of knots and plectonemes, the simulation traces from initially knotted configurations present more tangle events compared to initially unknotted ones (Fig. 18 of Ref. [46]).

Using our simulation setup, we can separate the effects of increasing torque and increasing driving force. Inspection of the simulation data reveals that, at a fixed pulling force, various regimes are observed as a function of the torque, Fig. 3(c). When the latter is sufficiently small, no plectoneme passages are recorded because the DNA twist accumulated on the *cis* side is limited, producing short and loose plectonemes that unravel before reaching the

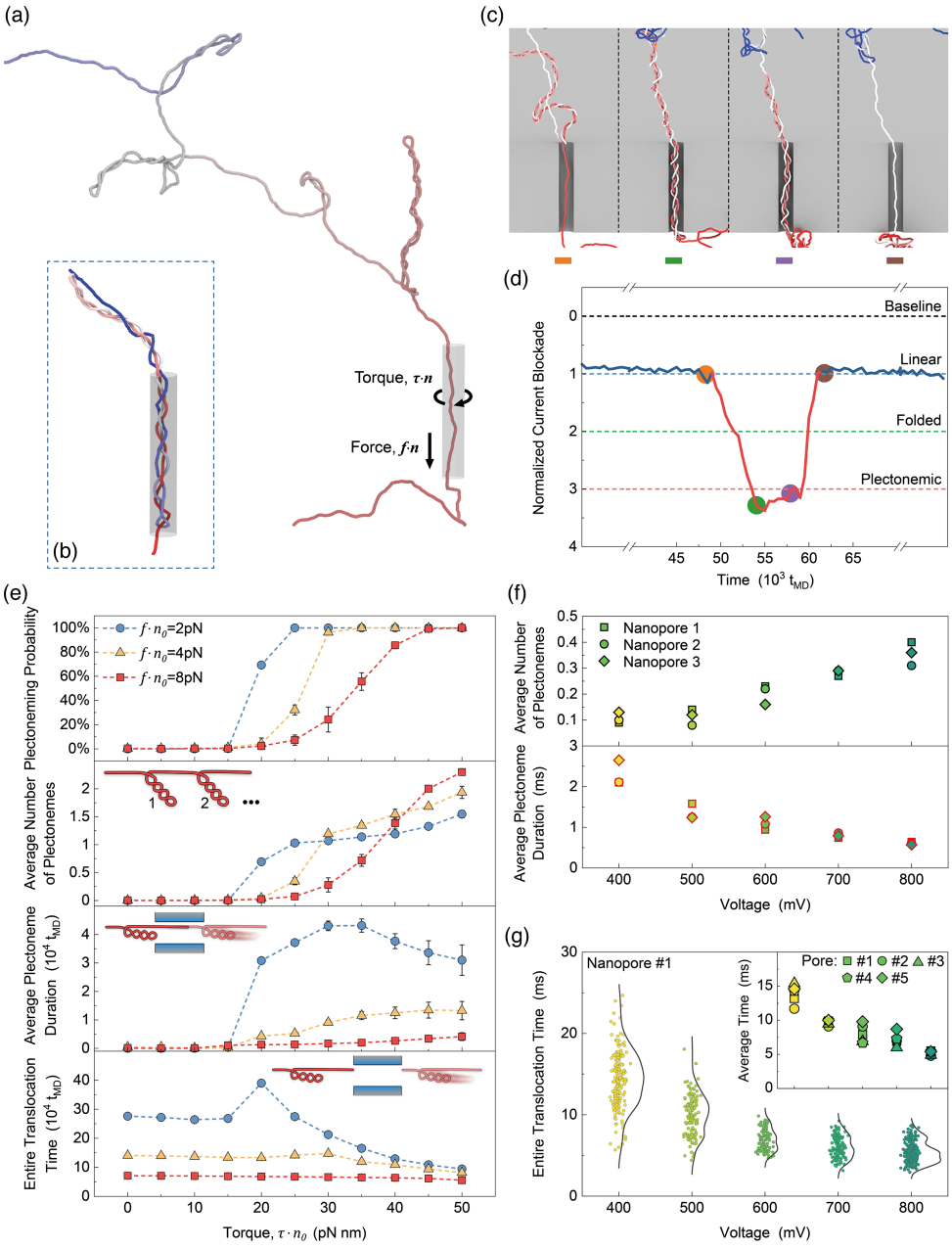

FIG. 3. Reproduction of plectoneme formation and translocation in molecular dynamics simulations. (a) Snapshot of an 8-kbp unknotted DNA chain translocating through a cylindrical pore (shaded cylinder) with a diameter of 14 nm and a length of 100 nm. Here, τ and f are, respectively, the torque per base pair and pulling force per base applied to the in-pore part of the DNA molecule. Their values are calibrated to previous electroosmosis-generated torque data in molecular dynamics simulations [26] and optical-tweezer-measured electrophoretic forces in conical nanopores [15], respectively (Note 7 of Ref. [46]). The total applied pulling force and torque are obtained by multiplying τ and f by the equivalent number of base pairs in the pore, n. (b) Snapshot of a plectoneme threading through the nanopore. (c) Snapshots of four stages of plectoneme translocation through the nanopore, from initial entry to complete exit. (d) Ionic current signal from plectoneme translocation, with four colored markers highlighting the corresponding stages in panel (c). Time is expressed in units of t_{MD}, the characteristic simulation time (Note 7 of Ref. [46]). (e) Plectoneme occurrence probability, average number of plectonemes, average duration of single plectoneme, and average duration of entire translocation time of all events as a function of the applied torque. The averages are taken over more than 250 independent initial configurations of unknotted and torsionally relaxed chains of 8-kbp length. For reference, the forces and torque reported in the graphs are multiplied by $n_0 = 300$, equivalent to the number of base pairs of a single dsDNA stretch inside the pore. (f) Average number of plectonemes and average duration of single plectoneme translocation event as a function of applied voltages derived from measurements of lambda DNA in three same-sized nanopores. (g) Entire translocation time of all events as a function of applied voltages from nanopore experiments. Each scatter point represents an individual event. The lines are half-violin distributions that fit the frequency of translocation time values. The inset is the average translocation time obtained from five same-sized nanopores.

pore entrance. However, as the torque reaches a certain threshold value, the plectonemes formed by the accumulation of twist become sufficiently complex and tightly wound that they can withstand the unraveling action of the propagating tension. These plectonemic structures are preserved as they pass through the pore, yielding the characteristic current drop. Note that the torque threshold for plectoneme passage grows with the pulling force because higher forces are more effective at plectoneme unraveling and thus higher twist rates are needed to observe plectoneme passages. As the torque increases, more plectoneme passages per trajectory are observed (second panel from the top). A noteworthy feature is that the passing plectonemes become longer as the twist is accumulated more rapidly. This feature is reflected in the duration of individual plectoneme events growing with applied moderate torque (third panel). However, because the total pulling force and torque grow extensively with the number of bases inside the pore, the passage of a long plectoneme can significantly speed up the translocation of the plectoneme and of the entire chain, too. This effect accounts for the decreasing trends observed at large torque for the entire translocation time and the single plectoneme duration at high force [Fig. 3(e), bottom panels].

Further parallels between the model and the actual system can be drawn by comparing the simulation data for 8-kbp DNA in Fig. 3(e) with the experimental measurements for lambda DNA in Figs. 3(f) and 3(g). Two key points should be taken into account for the comparison: (i) The relevant range of torque and pulling forces corresponds to 0.1–0.5 average number of plectonemes, hence in the proximity of the threshold torques, and (ii) unlike in the simulation setup, in experiments, the force and torque cannot be varied independently because they both vary with the applied voltage in an approximately linear fashion [26].

The experimental average number of plectoneme signals increases with voltage [Fig. 3(f), top], while their duration and the entire translocation decrease with voltage [Figs. 3(f) (bottom) and 3(g)]. All these qualitative features are reproduced by the simulation data. The average number of plectonemes increases both with force and torque and thus also for any of their linear combinations mimicking the effect of voltage increase. Analogous, concurrent, linear increases of force and torque result in decreasing durations of plectoneme events and of the entire trajectories (Fig. 19 of Ref. [46]), again in qualitative accordance with experiment.

Additional experiments and simulations examined the effect of nanopore size on the formation of plectonemes (Note 10 and Figs. 25–27 of Ref. [46]). The experimentally measured tangling probabilities at +800 mV for the two pore sizes (Fig. 25 of Ref. [46]) showed a higher tangling probability in the large pore. This trend is consistent with MD simulations, where larger pores display an increased probability of plectoneme formation under a given torque (Fig. 27 of Ref. [46]). Furthermore, the average number of plectonemes detected was greater for the larger pore [Fig. 27(b) of Ref. [46]]. A wider pore geometry facilitates plectoneme translocation, even discounting that larger nanopores result in larger electro-osmotic flow and generated torque. Analysis of average plectoneme duration and total translocation time [Figs. 27(c) and 27(d) of Ref. [46]] revealed no significant differences between the two pore sizes. These results collectively underscore the generality of our findings across a range of nanopore confinement regimes.

V. NICKS REDUCE PLECTONEME FORMATION

The simulations suggest that torsional rigidity of DNA is crucial for accumulating plectonemes that can withstand unraveling and pass through the pore. To test this idea, we designed three, different, same-length DNA nanostructures having different torsional constraints derived from M13mp18 DNA, including intact, nicked, and 1nt gap, Fig. 4(a). The intact one is a dsDNA (7228 bp) cut by restriction enzymes from the double-stranded M13mp18 vector having the phosphodiester bonds chemically linking all adjacent nucleotides. By contrast, the nicked and 1nt gap DNA have nicking sites evenly distributed along the length of the molecule. We use single-stranded M13mp18 DNA as a scaffold, then hybridize 190 oligonucleotide staples with complementary sequences, and thus produce a DNA construct (nicked) containing 189 nicking sites. Here, each staple contains 38 nucleotides [Fig. 4(b)]. The third 1nt gap construct is created by removing the last nucleotide in each staple, resulting in a one-nucleotide gap between every two adjacent staples (37 nucleotides). We note that the three types of DNA molecules are sequence identical and have the same length. Figure 4(c) schematically shows how the nicking sites hinder the propagation of torsion along the nanostructures. The prediction is that, without torsion propagation, the rotation is restricted up to the next nicking site, preventing the accumulation of significant twist and the formation of large plectonemes.

For a short DNA molecule like M13mp18 (7.2 kbp) that translocates much faster than lambda DNA (48.5 kbp), it is challenging to discriminate knots and plectonemes according to their duration (Figs. 15 and 16 of Ref. [46]). However, because the knotting probability of equilibrated chains depends on large-scale conformations and not on localized defects, the three DNA types are expected to have a similar number of knots. Thus, the overall tangling probability becomes a probe of how nicking affects plectoneme formation. Figure 4(d) shows the tangling probability for the three DNA nanostructures, along with another 8-kbp DNA of different sequences used as a control. As expected, the tangling probabilities of these three DNA types follow the order $P_{\text{intact}} > P_{\text{nicked}} > P_{1\,\text{nt gap}}$. The control 8-kbp DNA has a slightly higher tangling probability than the other three constructs, which we

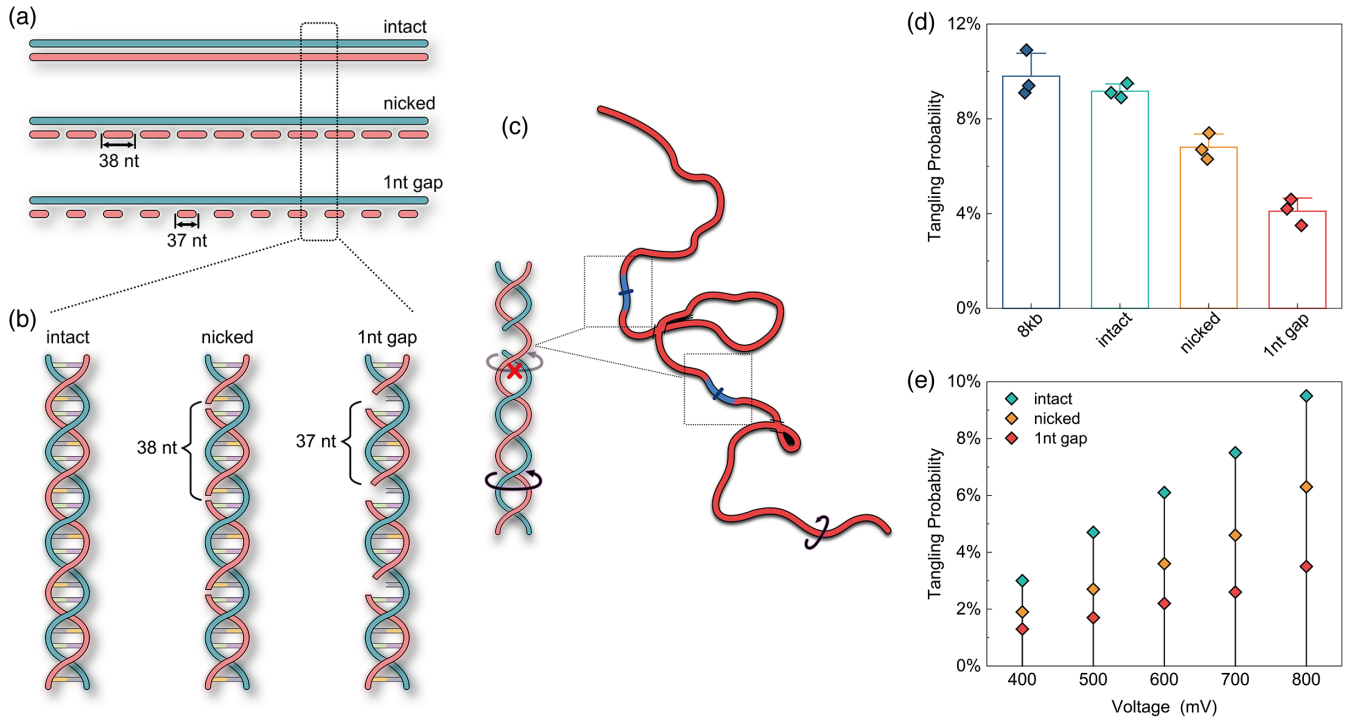

FIG. 4. Reduction of plectoneme formation resulting from torsion propagation hindrance. (a) Schematic of the intact M13mp18 DNA and the assembly of nicked and 1nt gap DNA constructs. The nicked and 1nt gap DNA constructs are synthesized by assembling 190 staples each containing either 38 or 37 nucleotides to the single-stranded M13mp18 scaffold, respectively. (b) Enlarged view of the helix structures of the three DNA types. The nicked construct has a phosphodiester bond break between each two staples (38 nucleotide distance) whereas the 1nt gap construct has an additional one-nucleotide gap in each break. (c) Schematic illustrating how nicking sites hinder the torsion propagation and thus prevent plectoneme formation. (d) Tangling probabilities of 8-kbp DNA, intact M13mp18 DNA, and nicked and 1nt gap DNA constructs measured in three nanopores. (e) Tangling probabilities of intact dsDNA, and nicked and 1nt gap DNA constructs as a function of voltage measured in the same pore.

attribute to the longer length of the former. Furthermore, we examine the voltage dependence of these three DNA types, as the formation of plectonemes is significantly affected by the voltage while that of knots is not. Figure 4(e) shows that the tangling probabilities of all three DNA types increase with the applied voltage from 400 mV to 800 mV, and, at each voltage, $P_{\text{intact}} > P_{\text{nicked}} > P_{1\text{ nt gap}}$. This voltage dependence further strengthens our conclusion that the torque is propagating along the molecule leading to the accumulation of DNA twist and the formation of plectonemes.

VI. CONCLUDING REMARKS

To conclude, we have demonstrated the presence of torsion propagation on the DNA polymer during its pore-translocation process. The DNA strand outside the nanopore is constantly rotated by this torsion and thus twisted into plectonemes. We use both experimental nanopore signals and molecular dynamics simulations as evidence that the configurated plectonemic structures can survive the unraveling action of the pulling force and translocate through the pore. The formation of plectonemes is strongly dependent on the torque applied on the DNA helix structure, which we show by the increasing overall tangling probability and number of plectonemes per event, both in experiments and simulations. Finally, we experimentally employ a nicking strategy to reduce torsion propagation and thereby hinder the formation of plectonemes.

The implications of our study are numerous. On the one hand, for the purpose of inferring the entangled state of DNA filaments *in vivo*, our results give a first proof-of-concept demonstration that the same nanopore setup can be used to concurrently detect plectonemes and knots and tell them apart. We recall that knots and plectonemes inevitably arise during the incessant *in vivo* DNA transactions effected by topoisomerase enzymes, which include strand passages, and DNA supercoiling and unzipping. Heretofore, these complex forms of DNA entanglement have been detected with electrophoretic techniques, which have been perfected to the point that *in vivo* supercoiling and knotting of circular eukaryotic chromosomes can be measured [59]. However, the complex interplay of the two types of entanglement on electrophoretic mobility requires distinct measurements for supercoiled and knotted states and an irreversible intervening DNA manipulation: In fact, knots can be reliably detected only after DNA torsion is fully relaxed by nicking. Our results indicate that this limitation

could be overcome by resorting to nanopore-based setups, thanks to the different duration of the current signals of knots and plectonemes. Obtaining the joint probability distribution of knots and plectonemes *in vivo* would take the characterization of topoisomerase actions to an entirely new level, with significant implications for advancing the current understanding of these enzymes. Furthermore, our observation of nick-reduced plectoneme formation suggests that nanopores may serve as a tool for detecting DNA damage, with plectoneme formation probabilities providing a measure of DNA integrity. By adjusting nanopore parameters, it may be possible to further enhance sensitivity to DNA damage.

On the other hand, for the purpose of biomolecule sensing, the conformational motifs such as folds, knots, and plectonemes are not desired as they create complex signals that overlap the information of biopolymers. For instance, knots and plectonemes generate similar current drops as the encoded DNA nanostructures [28] on the polymer scaffold and thus reduce the detection efficiency. In both cases, our work suggests ways to either avoid introducing spurious plectonemic signals or maintain a certain torque threshold to detect them.

It is an interesting question if minimization of the electro-osmotic flow will prevent torque and hence formation of plectonemes or rather reduce their detection as they do not reach the nanopores. In any case, the realization of the importance of torque will allow one to tune the solution properties and voltage to optimize the measurements for the respective question. Moreover, as the formation of plectonemes relies on the dynamics of DNA segments outside the pore, accelerating the polymer translocation speed inside the nanopore can likely reduce the plectoneme size as well as their occurrence. In addition, given that we have proven that the nicking strategy significantly inhibits plectoneme formation, nicks can be introduced to the DNA polymer as an alternative strategy.

Vice versa, we have demonstrated that tuning the solution properties or the charge density of the nanopore surface can induce a supercoiled state, and with sufficient torque, this state can be maintained and detected as the DNA is pulled into the widening conical pore. Our system represents a viable proxy for studying the extrusion of supercoiled DNA [6].

In our voltage-driven setup, the nanopore provides both the torque and force necessary for plectoneme formation and subsequent translocation while also functioning as a sensor of these events. The confined geometry empowers these processes by the elevated electric field within it; thus, the pore diameter affects the torque, driving plectoneme initiation and the pulling force threading plectonemes through the pore. The magnitude of the electroosmotic flow both increases the torque on the DNA in a nanopore and reduces the effective net force, driving the DNA through the nanopore; nanopores that create stronger electro-osmotic effects are also more conducive to plectoneme formation in translocating DNA filaments. We also note that, in nonconfined physiological environments, flows generated by pressure or salinity gradients can likewise impart rotational motion to DNA, potentially promoting plectoneme formation.

From a physics-based perspective, our work reveals that the formation of plectonemes depends on several conditions. First, it is the torque that originates from the interaction between the electro-osmotic flow and the DNA helix. This helix structure holds significance in the rotation behavior and subsequent dynamics of the DNA strand outside the nanopore. Apart from the right-handed helix (B-form) used here, left-handed helix DNA was reported to rotate in an opposite direction in simulations [26], while A-form RNA experiences slower rotation than B-form DNA due to its different helix shape [26]. These rotational differences should have profound influence on the formation of plectonemes. Second, translocation timescale and polymer length are crucial for the occurrence of the plectoneme and its size. Longer DNA polymers are more likely to form large-sized plectonemes as their cis segments have more time to evolve into plectonemic structures. Additionally, longer polymers feature extended relaxation times, which changes the probability for plectonemes to maintain the structure outside the nanopore.

Both polymer translocation and rotation are out-of-equilibrium processes. From the perspective of energy dissipation during these processes, we show that the torsion propagation outward from the nanopore is another important pathway to dissipate the energy stemming from the applied transmembrane potential. Our work emphasizes that the dynamics of the in-pore strand is tightly linked to that of the cis part, by both tension and torsion propagation.

By demonstrating and detecting torsion-driven plectoneme formation in DNA filaments, our study opens new perspectives for detailed studies of DNA plectonemes and supercoiling. The advantage of our method is that, in nanopores, torque is applied locally on the molecules in a voltage-dependent manner. Possible research areas include the analysis of genome compactification and organization to the prevention of entanglement, the influence on topoisomerase activity, and gene regulation.

These evolutionarily selected functions hinge on DNA behaving as a reconfigurable twistable DNA chain, a property largely absent in naturally occurring RNA and proteins, whose functionality typically relies on maintaining specific folded structures. At the same time, we envisage that it may be possible in the future to engineer sufficiently long polyelectrolytes that have DNA-like twistability and bending rigidity. Such a system would be addressable by our setup, making it possible to investigate out-of-equilibrium torsional responses across a broader range of mechanical parameters than those of DNA.

ACKNOWLEDGMENTS

F. Z. and U. F. K. acknowledge funding from an ERC Proof of Concept Grant (PoreDetect 899538) and an ERC consolidator grant (Designerpores 647144). F. Z. acknowledges funding from the China Scholarship Council (202106090221). U. F. K. acknowledges UK Research and Innovation (UKRI) under the UK government's Horizon Europe funding guarantee EP/X023311/1. M. A. was supported by the UK Engineering and Physical Sciences Research Council (EPSRC) Grant No. EP/S023046/1 for the Sensor CDT. M. A. acknowledges funding from a UKSACB scholarship. C. Mi. acknowledges funding from MUR Grant No. PRIN-2022R8YXMR and PNRR Grant No. CN_00000013_CN-HPC, M4C2I1.4, spoke 7, funded by NextGenerationEU. C. Ma. and A. A. acknowledge funding from the Human Frontier Science Project (RGP0047/2020) and the National Science Foundation (ID-2411133). J. S. acknowledges funding from National Natural Science Foundation of China (52075099, 52361145851). We thank Qing Zhao, Rui Hu, and Zhan Wang for their assistance with the TEM fabrication of cylindrical nanopores.

U. F. K., C. Mi., and A. A. conceived the concept of plectoneme formation during nanopore translocation. F. Z. and M. A. conducted the nanopore experiments. K. C. performed the FEM simulations. J. S. fabricated the Si_3N_4 membrane chips. F. Z. wrote the data analysis scripts with input from M. A. F. Z. and U. F. K. analyzed the experimental data. A. S. and C. Mi. performed DNA analysis of the Monte Carlo and molecular dynamics simulations. C. Ma. and A. A. performed the ionic current analysis of the molecular dynamics trajectories. All authors discussed the findings and co-wrote the manuscript.

The authors declare no competing interests.

[1] Y.-L. Ying, Z.-L. Hu, S. Zhang, Y. Qing, A. Fragasso, G. Maglia, A. Meller, H. Bayley, C. Dekker, and Y.-T. Long, *Nanopore-based technologies beyond DNA sequencing*, Nat. Nanotechnol. **17**, 1136 (2022).

[2] L. Xue, H. Yamazaki, R. Ren, M. Wanunu, A. P. Ivanov, and J. B. Edel, *Solid-state nanopore sensors*, Nat. Rev. Mater. **5**, 931 (2020).

[3] M. Vayssières, N. Marechal, L. Yun, B. L. Duran, N. K. Murugasamy, J. M. Fogg, L. Zechiedrich, M. Nadal, and V. Lamour, *Structural basis of DNA crossover capture by Escherichia Coli DNA gyrase*, Science **384**, 227 (2024).

[4] K. Coshic, C. Maffeo, D. Winogradoff, and A. Aksimentiev, *The structure and physical properties of a packaged bacteriophage particle*, Nature (London) **627**, 905 (2024).

[5] M. Zhang, R. Nixon, F. Schaufelberger *et al.*, *Mechanical scission of a knotted polymer*, Nat. Chem. **16**, 1366 (2024).

[6] E. Kim, A. M. Gonzalez, B. Pradhan, J. van der Torre, and C. Dekker, *Condensin-driven loop extrusion on supercoiled DNA*, Nat. Struct. Mol. Biol. **29**, 719 (2022).

[7] J. Lee, M. Wu, J. T. Inman *et al.*, *Chromatinization modulates topoisomerase II processivity*, Nat. Commun. **14**, 6844 (2023).

[8] A. L. Pyne, A. Noy, K. H. Main *et al.*, *Base-pair resolution analysis of the effect of supercoiling on DNA flexibility and major groove recognition by triplex-forming oligonucleotides*, Nat. Commun. **12**, 1053 (2021).

[9] A. D. Bates and A. Maxwell, *DNA Topology* (Oxford University Press, USA, 2005).

[10] A. Dorey and S. Howorka, *Nanopore DNA sequencing technologies and their applications towards single-molecule proteomics*, Nat. Chem. **16**, 314 (2024).

[11] E. A. Manrao, I. M. Derrington, A. H. Laszlo, K. W. Langford, M. K. Hopper, N. Gillgren, M. Pavlenok, M. Niederweis, and J. H. Gundlach, *Reading DNA at single-nucleotide resolution with a mutant MspA nanopore and phi29 DNA polymerase*, Nat. Biotechnol. **30**, 349 (2012).

[12] G. M. Cherf, K. R. Lieberman, H. Rashid, C. E. Lam, K. Karplus, and M. Akeson, *Automated forward and reverse ratcheting of DNA in a nanopore at 5-Å precision*, Nat. Biotechnol. **30**, 344 (2012).

[13] I. M. Derrington, J. M. Craig, E. Stava *et al.*, *Subangstrom single-molecule measurements of motor proteins using a nanopore*, Nat. Biotechnol. **33**, 1073 (2015).

[14] K. Chen, I. Jou, N. Ermann, M. Muthukumar, U. F. Keyser, and N. A. W. Bell, *Dynamics of driven polymer transport through a nanopore*, Nat. Phys. **17**, 1043 (2021).

[15] N. A. Bell, K. Chen, S. Ghosal, M. Ricci, and U. F. Keyser, *Asymmetric dynamics of DNA entering and exiting a strongly confining nanopore*, Nat. Commun. **8**, 380 (2017).

[16] C.-Y. Lin, R. Fotis, Z. Xia, K. Kavetsky, Y.-C. Chou, D. J. Niedzwiecki, M. Biondi, F. Thei, and M. Drndić, *Ultrafast polymer dynamics through a nanopore*, Nano Lett. **22**, 8719 (2022).

[17] J. Li, M. Gershow, D. Stein, E. Brandin, and J. A. Golovchenko, *DNA molecules and configurations in a solid-state nanopore microscope*, Nat. Mater. **2**, 611 (2003).

[18] W. Reisner, K. J. Morton, R. Riehn, Y. M. Wang, Z. Yu, M. Rosen, J. C. Sturm, S. Y. Chou, E. Frey, and R. H. Austin, *Statics and dynamics of single DNA molecules confined in nanochannels*, Phys. Rev. Lett. **94**, 196101 (2005).

[19] Y. Qi, L. Zeng, A. Khorshid, R. J. Hill, and W. W. Reisner, *Compression of nanoslit confined polymer solutions*, Macromolecules **51**, 617 (2018).

[20] A. Khorshid, S. Amin, Z. Zhang, T. Sakaue, and W. W. Reisner, *Nonequilibrium dynamics of nanochannel confined DNA*, Macromolecules **49**, 1933 (2016).

[21] N. Ermann, N. Hanikel, V. Wang, K. Chen, N. E. Weckman, and U. F. Keyser, *Promoting single-file DNA translocations through nanopores using electro-osmotic flow*, J. Chem. Phys. **149**, 163311 (2018).

[22] R. Kumar Sharma, I. Agrawal, L. Dai, P. S. Doyle, and S. Garaj, *Complex DNA knots detected with a nanopore sensor*, Nat. Commun. **10**, 4473 (2019).

[23] K. Briggs, G. Madejski, M. Magill, K. Kastritis, H. W. de Haan, J. L. McGrath, and V. Tabard-Cossa, *DNA*

translocations through nanopores under nanoscale preconfinement, Nano Lett. **18**, 660 (2018).
[24] B. N. Anderson, M. Muthukumar, and A. Meller, *pH tuning of DNA translocation time through organically functionalized nanopores*, ACS Nano **7**, 1408 (2013).
[25] X. Shi, A.-K. Pumm, C. Maffeo *et al.*, *A DNA turbine powered by a transmembrane potential across a nanopore*, Nat. Nanotechnol. **19**, 338 (2024).
[26] C. Maffeo, L. Quednau, J. Wilson, and A. Aksimentiev, *DNA double helix, a tiny electromotor*, Nat. Nanotechnol. **18**, 238 (2023).
[27] X. Shi, A.-K. Pumm, J. Isensee, W. Zhao, D. Verschueren, A. Martin-Gonzalez, R. Golestanian, H. Dietz, and C. Dekker, *Sustained unidirectional rotation of a self-organized DNA rotor on a nanopore*, Nat. Phys. **18**, 1105 (2022).
[28] F. Zheng, M. Alawami, J. Zhu, C. M. Platnich, J. Sha, U. F. Keyser, and K. Chen, *DNA carrier-assisted molecular ping-pong in an asymmetric nanopore*, Nano Lett. **23**, 11145 (2023).
[29] C. Plesa, L. Cornelissen, M. W. Tuijtel, and C. Dekker, *Non-equilibrium folding of individual DNA molecules recaptured up to 1000 times in a solid state nanopore*, Nanotechnology **24**, 475101 (2013).
[30] M. Mihovilovic, N. Hagerty, and D. Stein, *Statistics of DNA capture by a solid-state nanopore*, Phys. Rev. Lett. **110**, 028102 (2013).
[31] J. Sarabadani, T. Ikonen, and T. Ala-Nissila, *Iso-flux tension propagation theory of driven polymer translocation: The role of initial configurations*, J. Chem. Phys. **141**, 214907 (2014).
[32] V. V. Palyulin, T. Ala-Nissila, and R. Metzler, *Polymer translocation: The first two decades and the recent diversification*, Soft Matter **10**, 9016 (2014).
[33] J. Sarabadani, T. Ikonen, and T. Ala-Nissila, *Theory of polymer translocation through a flickering nanopore under an alternating driving force*, J. Chem. Phys. **143**, 074905 (2015).
[34] J. Sarabadani and T. Ala-Nissila, *Theory of pore-driven and end-pulled polymer translocation dynamics through a nanopore: An overview*, J. Phys. Condens. Matter **30**, 274002 (2018).
[35] T. Ikonen, A. Bhattacharya, T. Ala-Nissila, and W. Sung, *Influence of non-universal effects on dynamical scaling in driven polymer translocation*, J. Chem. Phys. **137**, 085101 (2012).
[36] C. Plesa, D. Verschueren, S. Pud, J. van der Torre, J. W. Ruitenberg, M. J. Witteveen, M. P. Jonsson, A. Y. Grosberg, Y. Rabin, and C. Dekker, *Direct observation of DNA knots using a solid-state nanopore*, Nat. Nanotechnol. **11**, 1093 (2016).
[37] L. Olavarrieta, P. Hernandez, D. B. Krimer, and J. B. Schvartzman, *DNA knotting caused by head-on collision of transcription and replication*, J. Mol. Biol. **322**, 1 (2002).
[38] R. W. Deibler, J. K. Mann, D. W. L. Sumners *et al.*, *Hin-mediated DNA knotting and recombining promote replicon dysfunction and mutation*, BMC Mol. Biol. **8**, 44 (2007).
[39] J. Portugal and A. Rodríguez-Campos, *T7 RNA polymerase cannot transcribe through a highly knotted DNA template*, Nucleic Acids Res. **24**, 4890 (1996).
[40] A. Valdés, J. Segura, S. Dyson , B. Martínez-García, and J. Roca, *DNA knots occur in intracellular chromatin*, Nucleic Acids Res. **46**, 650 (2018).
[41] A. Suma and C. Micheletti, *Pore translocation of knotted DNA rings*, Proc. Natl. Acad. Sci. U.S.A. **114**, E2991 (2017).
[42] C. Micheletti and E. Orlandini, *Knotting and unknotting dynamics of DNA strands in nanochannels*, ACS Macro Lett. **3**, 876 (2014).
[43] L. Coronel, A. Suma, and C. Micheletti, *Dynamics of supercoiled DNA with complex knots: Large-scale rearrangements and persistent multi-strand interlocking*, Nucleic Acids Res. **46**, 7533 (2018).
[44] A. R. Klotz, B. W. Soh, and P. S. Doyle, *Motion of knots in DNA stretched by elongational fields*, Phys. Rev. Lett. **120**, 188003 (2018).
[45] R. K. Sharma, I. Agrawal, L. Dai, P. Doyle, and S. Garaj, *DNA knot malleability in single-digit nanopores*, Nano Lett. **21**, 3772 (2021).
[46] See Supplemental Material at http://link.aps.org/supplemental/10.1103/spyg-kl86 for methods and supporting data.
[47] E. Uehara, L. Coronel, C. Micheletti, and T. Deguchi, *Bimodality in the knotting probability of semiflexible rings suggested by mapping with self-avoiding polygons*, React. Funct. Polym. **134**, 141 (2019).
[48] L. Tubiana, A. Rosa, F. Fragiacomo, and C. Micheletti, *Spontaneous knotting and unknotting of flexible linear polymers: Equilibrium and kinetic aspects*, Macromolecules **46**, 3669 (2013).
[49] S. Amin, A. Khorshid, L. Zeng, P. Zimny, and W. Reisner, *A nanofluidic knot factory based on compression of single DNA in nanochannels*, Nat. Commun. **9**, 1506 (2018).
[50] A. Khorshid, P. Zimny, D. Tétreault-La Roche, G. Massarelli, T. Sakaue, and W. Reisner, *Dynamic compression of single nanochannel confined DNA via a nanodozer assay*, Phys. Rev. Lett. **113**, 268104 (2014).
[51] A. Rosa, M. Di Ventra, and C. Micheletti, *Topological jamming of spontaneously knotted polyelectrolyte chains driven through a nanopore*, Phys. Rev. Lett. **109**, 118301 (2012).
[52] Y. A. Fosado, D. Michieletto, C. A. Brackley, and D. Marenduzzo, *Nonequilibrium dynamics and action at a distance in transcriptionally driven DNA supercoiling*, Proc. Natl. Acad. Sci. U.S.A. **118**, e1905215118 (2021).
[53] N. Laohakunakorn, V. V. Thacker, M. Muthukumar, and U. F. Keyser, *Electroosmotic flow reversal outside glass nanopores*, Nano Lett. **15**, 695 (2015).
[54] N. Laohakunakorn and U. F. Keyser, *Electroosmotic flow rectification in conical nanopores*, Nanotechnology **26**, 275202 (2015).
[55] G. Chirico and J. Langowski, *Kinetics of DNA supercoiling studied by Brownian dynamics simulation*, Biopolymers **34**, 415 (1994).
[56] C. A. Brackley, A. N. Morozov, and D. Marenduzzo, *Models for twistable elastic polymers in Brownian dynamics, and their implementation for LAMMPS*, J. Chem. Phys. **140**, 135103 (2014).
[57] J. Wilson, K. Sarthak, W. Si, L. Gao, and A. Aksimentiev, *Rapid and accurate determination of nanopore ionic*

current using a steric exclusion model, ACS Sens. **4**, 634 (2019).

[58] A. Choudhary, C. Maffeo, and A. Aksimentiev, *Multi-resolution simulation of DNA transport through large synthetic nanostructures*, Phys. Chem. Chem. Phys. **24**, 2706 (2022).

[59] A. Valdés, L. Coronel, B. Martínez-García, J. Segura, S. Dyson, O. Díaz-Ingelmo, C. Micheletti, and J. Roca, *Transcriptional supercoiling boosts topoisomerase II-mediated knotting of intracellular DNA*, Nucleic Acids Res. **47**, 6946 (2019).